Invited Paper

Development of high-frequency cw gyrotrons for DNP/NMR applications

Monica Blank [1*], Philipp Borchard [1], Stephen Cauffman [1], Kevin Felch [1], Melanie Rosay [2] , and Leo Tometich [2]

[1] Communications and Power Industries, 811 Hansen Way, Palo Alto, CA 94304, USA

[2] Bruker-Biospin, 15 Fortune Drive, Billerica, MA 01730, USA

[*] Email: monica.blank@cpii.com

(Received 22 December 2016)

Abstract: Dynamic nuclear polarization (DNP) enhanced nuclear magnetic resonance (NMR) spectroscopy is an emerging and growing application for high-frequency, continuous-wave (cw) gyrotrons. For DNP, gyrotrons capable of producing tens to hundreds of watts at millimeter-wave and terahertz frequencies are required. As an original equipment manufacturer of gyrotrons for Bruker Biospin DNP/NMR spectrometers, CPI has developed cw gyrotrons at 263*GHz*, 395*GHz*, and 527*GHz*, all of which are capable of producing at least 50 *W* output power. The gyrotrons at all three frequencies operate at the second harmonic of the cyclotron frequency and produce high-quality Gaussian output beams suitable for transmission in corrugated waveguides. To date, 30 Bruker DNP/NMR systems using CPI gyrotrons have been installed around the world. Key features of the gyrotrons, as well as the results of experimental demonstrations, are presented.

Keywords: gyrotron, millimeter wave, terahertz, DNP, NMR spectroscopy

doi: 10.11906/TST.177-186.2016.12.17

1. Introduction

Recently, a renewed and growing interest in dynamic nuclear polarization (DNP) enhanced nuclear magnetic resonance (NMR) spectroscopy has driven the development of high-frequency, low and moderate-power, continuous wave (cw) gyrotrons. Although solid state NMR is a widely used and powerful spectroscopic method, its inherent low sensitivity can limit its efficacy for some applications. DNP, which is one of several techniques used to enhance the sensitivity of high frequency NMR, involves the transfer of the large polarization present in the electron spin reservoir of a sample, normally doped with a paramagnetic polarizing agent, to the nuclear spins via the irradiation of the sample with millimeter or terahertz waves. Generally, tens or hundreds of watts of power at the source is required for optimal DNP enhancement at NMR frequencies in the range of 400-900*MHz* and beyond. Although solid-state and slow-wave devices are available and have been used for DNP at millimeter wave frequencies, gyrotrons are generally more capable of producing moderate output powers at high frequencies than other device types and are, therefore, of particular interest as DNP sources.

In the past several decades, following the pioneering work at the Massachusetts Institute of Technology [1, 2], research efforts in the design, development, and implementation of gyrotrons in DNP/NMR systems have been carried out at several institutions around the world [3-8]. The success of these numerous research efforts in proving the significant NMR signal enhancements capabilities, often in excess of 100, ultimately led to development of commercial gyrotron-based DNP systems [9-11].

A schematic diagram of a typical commercial gyrotron-based solid-state DNP/NMR system is shown in Figure 1. The system consists of an NMR spectrometer, including a superconducting magnet, low-temperature magic-angle-spinning DNP/NMR probe, and NMR control system; a gyrotron and dedicated magnet, along with a power supply/control system; and a transmission line to connect the gyrotron source to the DNP/NMR probe.

CPI, as an original equipment manufacturer of gyrotrons for Bruker DNP systems, has developed cw gyrotrons capable of producing at least 50*W* output power at 263 *GHz*, 395 *GHz*, and 527*GHz*. To date, CPI has built and delivered 32 gyrotrons for Bruker DNP spectrometers, including fifteen at 263*GHz*, twelve at 395*GHz*, and five at 527*GHz*. Below, in Section 2, the basic design and key features of the gyrotrons at 263*GHz*, 395*GHz*, and 527*GHz* will be detailed. In Section 3, the results of experimental demonstrations of the gyrotrons will be described and in Section 4, summary conclusions will be made.

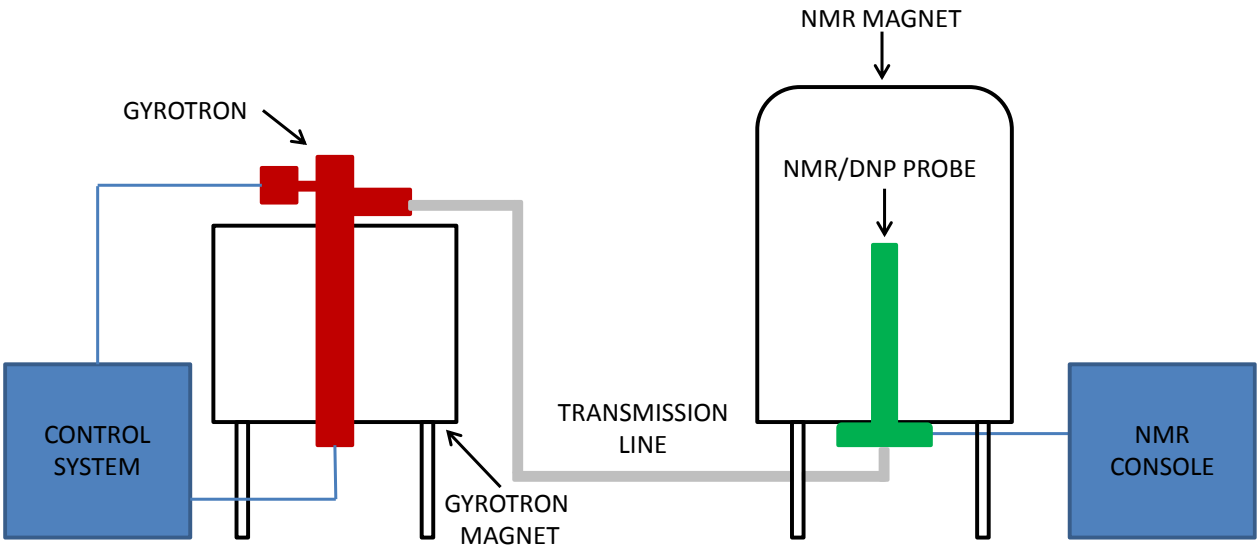

Fig. 1 Schematic diagram of typical commercial soid-state DNP/NMR system.

2. Key features of the 263 GHz, 395 GHz, and 527 GHz gyrotrons

A solid model of the 263GHz gyroton is shown in Figure 2. The mechanical design and key features of the 395*GHz* and 527*GHz* gyrotrons are very similar to those of the 263*GHz* gyrotron

depicted in the figure. All three gyrotrons are designed to stably produce at least 50*W* of output power at their respective frequencies. Each makes use of a distinct single-anode magnetron injection gun, designed to operate at voltages from 15-20*kV* and beam currents up to 200*mA*. The electron beam is transported from the gun to the interaction cavity through a beam tunnel, which includes alternating rings of lossy ceramic and copper to inhibit any possible RF generation. As the electron beam travels along the beam tunnel toward the interaction cavity, it is compressed by the increasing magnetic field of the superconducting magnet. The emitter size and compression ratio, which are not the same for the 263*GHz*, 395*GHz*, and 527*GHz* gyrotons, are carefully selected to ensure that the beam size in the interaction cavity is optimal for the chosen mode.

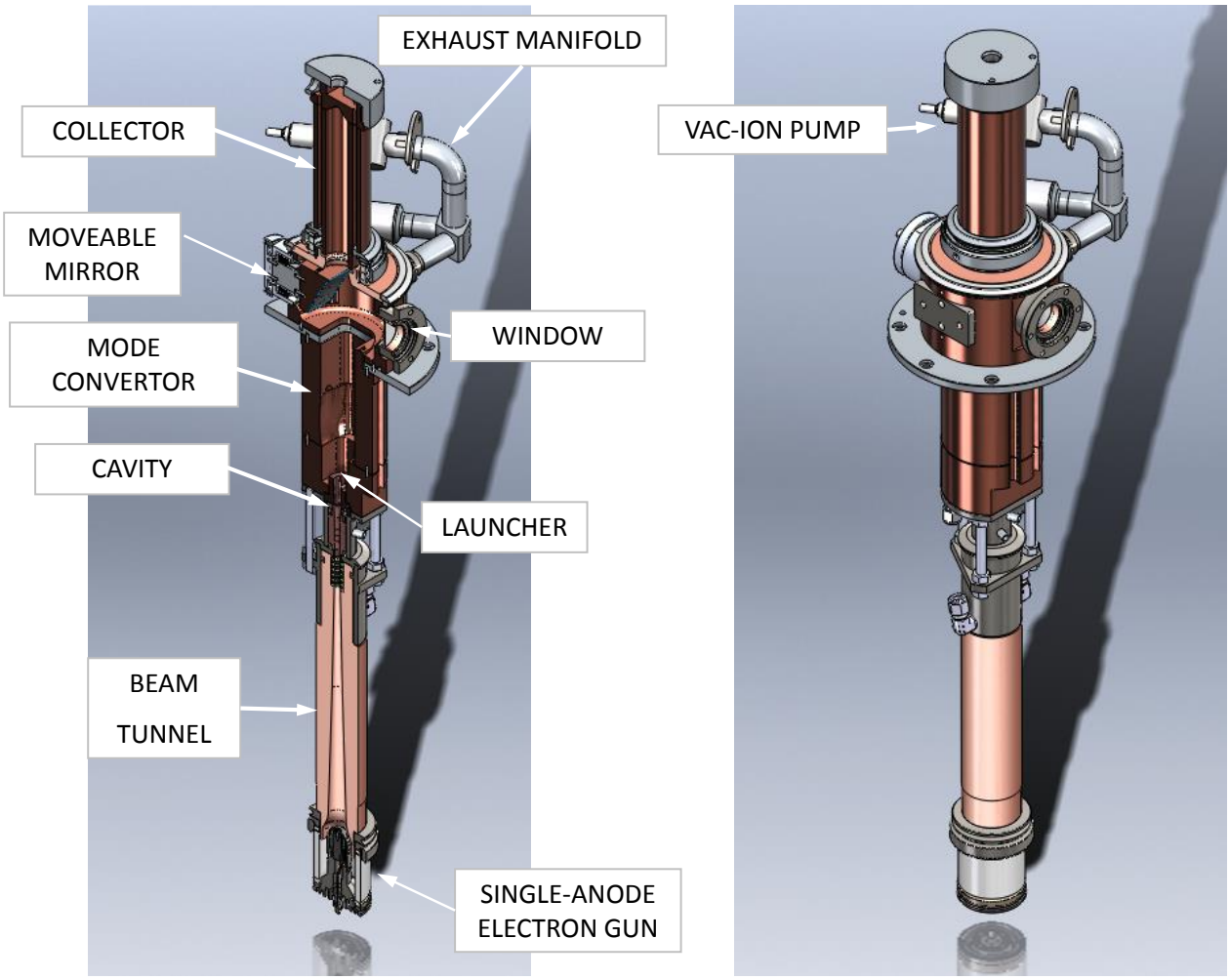

Fig. 2 Solid model of the 263*GHz* gyrotron with key features highlighted.

The 263*GHz* gyrotron operates in the second harmonic $TE_{11,2}$ mode at 4.9*T*. The 395*GHz* and 527*GHz* gyrotrons operate in the second harmonic $TE_{10,3}$ and $TE_{14,3}$ modes, respectively, at 7.2*T* and 9.7*T*. In all three cases, the operating modes are converted to high-quality Gaussian beams with a launcher and a series of mirrors that both transport and shape the output beam, similar to

the mode converter described in [12]. The shape of the launcher, which has shallow wall deformations designed to create a mode mix that transforms the operating mode to a beam with a Gaussian field profile, is numerically optimized to maximize the desired Gaussian mode content of the launched beam. Four mirrors are then used to shape the launched beam into a beam with waist size and waist position optimized for transport through the window and injection into a corrugated waveguide, 19*mm* diameter in the case of the 263*GHz* gyrotron and 16*mm* diameter for the 395 and 527*GHz* gyrotrons. The final mirror in the system is adjustable so that the output beam can be positioned in the center of the Al_2O_3 output window and aligned for optimal coupling to the corrugated waveguide during operation.

The spent electron beam is then deposited on the walls of the collector, which is identical for the three gyrotrons. A 2*l/s* vacion pump is used during gyrotron operation. The orientation and position of the vacion pump are designed to use the fringing field of the superconducting magnet, not a permanent magnet, for proper pump operation.

A photograph of the 395*GHz* gyrotron (left) and 527*GHz* gyrotron (right) is shown in Figure 3.

Fig. 3 Photograph of the 395*GHz* gyrotron, on the left, and the 527*GHz* gyrotron, on the right.

3. Experimental results

Figure 4 shows a photograph of the 395*GHz* gyrotron being tested in the Bruker superconducting magnet at CPI. A calorimetric load, positioned at the end of one section of corrugated waveguide, is used to measure power during the tests.

Typical measured parameter variation curves for the gyrotrons at 263*GHz*, 395*GHz*, and 527*GHz* are plotted in Figures 5 and 6. As shown in Figure 5, for each of the three gyrotrons the output power can be smoothly varied from over 50*W*, the required power, to less than 5*W* by varying voltage. For the measurements, the beam current is held fixed at 100*mA*, 140*mA*, and 130*mA* for the 263*GHz*, 395*GHz*, and 527*GHz* gyrotrons, respectively. At 17.4*kV* and 100*mA*, the 263*GHz* gyrotron generates 109*kW*, corresponding to 10.9% efficiency. The efficiencies of the 395*GHz* and 527*GHz* gyrotrons at the highest power points in Figure 5 are 2.5% and 2.2%, respectively.

In Figure 6, typical values of measured output power versus beam current with beam voltage held fixed are plotted for each of the three gyrotrons. As shown in the figure, for the 263*GHz* gyrotron output power varies from 89*W* to 7 *W* as the beam current is reduced from 178*mA* to 71*mA* with the beam voltage held constant at 16.5*kV*. Similarly, the 395*GHz* gyrotron output power varies from 80*W* to 11*W* at 17.4*kV* as the beam current is reduced from 178 to 93*mA*, and the 527*GHz* gyrotron power at 17.5*kV* beam voltage varies from 60*W* to 8*W* as the beam current varies from 178 to 106*mA*.

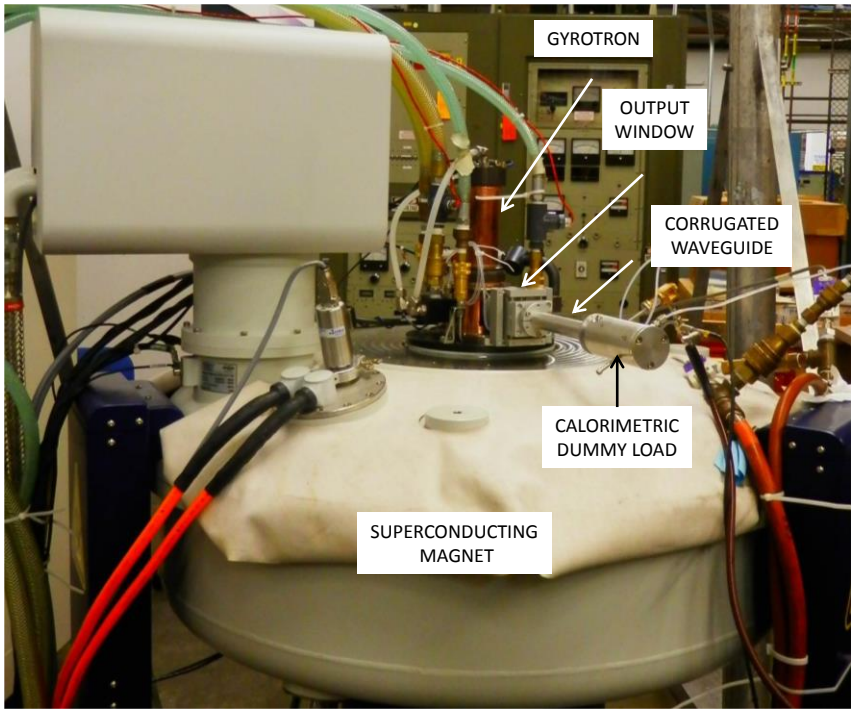

Fig. 4 Photograph of the 395*GHz* gyrotron in test. A calorimetric dummy load, positioned at the end of a section of 16-*mm* diameter corrugated waveguide, is used for power measurements.

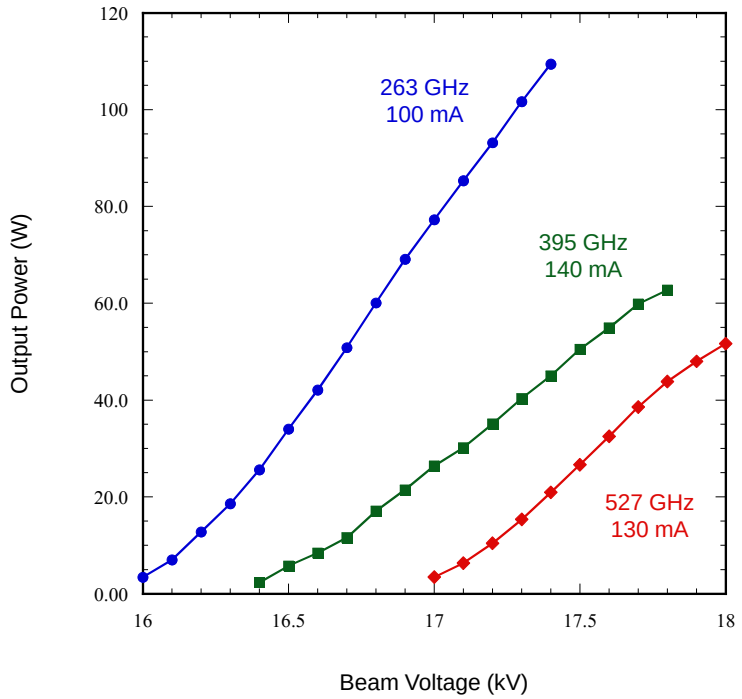

Fig. 5 Measured output power versus beam voltage for the 263*GHz* gyrotron operating at 100*mA* beam current (filled circles), the 395*GHz* gyrotron operating at 140*mA* (filled squares), and the 527*GHz* gyrotron operating at 130*mA* (filled diamonds).

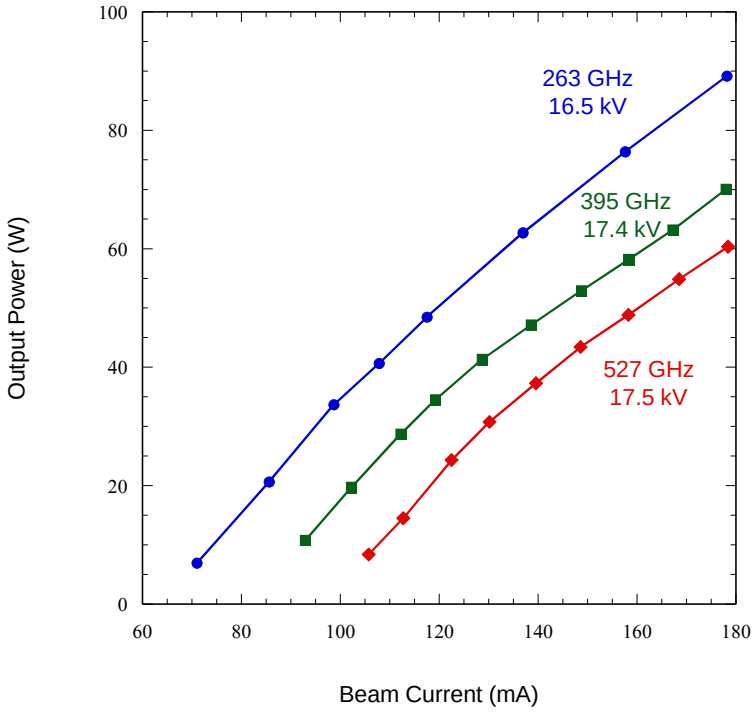

Fig. 6 Measured output power versus beam current for the 263*GHz* gyrotron operating at 16.5*kV* beam voltage (filled circles), the 395*GHz* gyrotron operating at 17.4 *kV*(filled squares), and the 527*GHz* gyrotron operating at 17.5*kV* (filled diamonds).

In addition to parameter variation curves, infrared images of the output beam are made for each gyrotron to determine the quality of the Gaussian beam. Figure 7 shows the setup for the infrared image measurement. The beam is incident on a paper target which is laser-aligned with the section of corrugated waveguide. The target is moved in a direction perpendicular to the waveguide and images of the beam at several points along the propagation path are made. The infrared data is then analyzed, with the assumption that the measured temperature is proportional to the square of the electric field, and comparisons to the desired Gaussian beam shape are made.

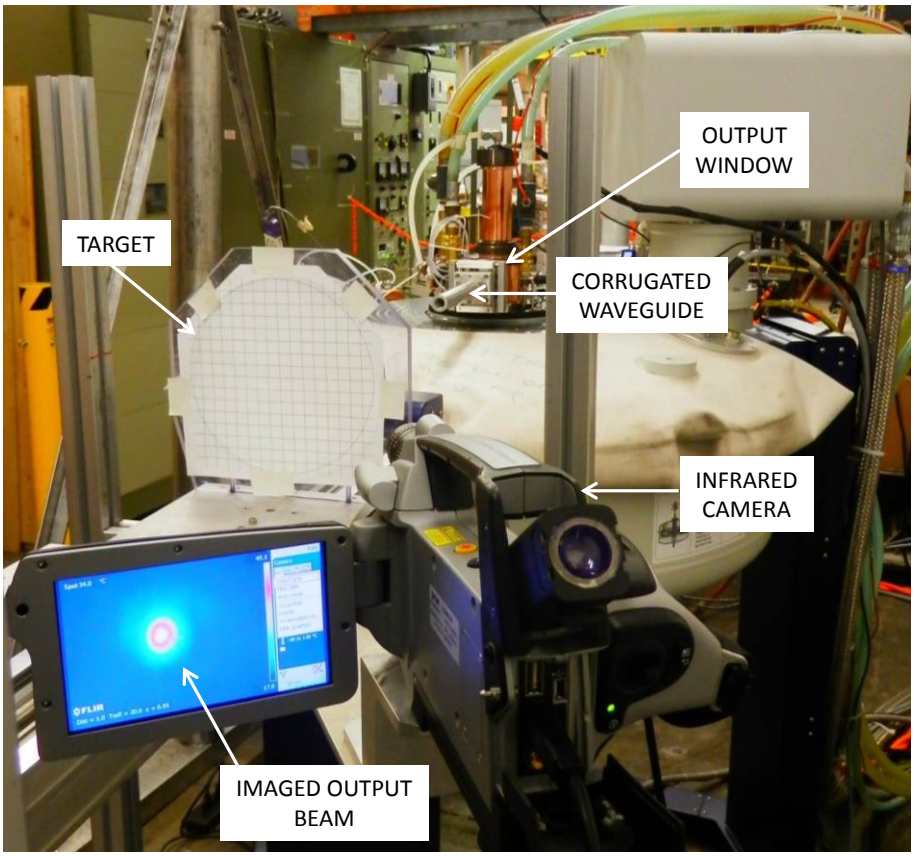

Fig. 7 Photograph showing the test set-up for infrared measurements of the output beam. The beam is incident on a paper target that is laser-aligned with the waveguide.

Figure 8 shows typical images of the beam along the propagation path for the 527*GHz* gyrotron. In the figure, the distance from the output guide is indicated at the top of each image. The crosshairs represent the position of the waveguide center and the circle is 5.08*cm* in diameter. As is evident from the figure, the gyrotron produces a high-quality Gaussian beam which is centered with and travelling perpendicular to the corrugated waveguide. Figure 9 shows the measured horizontal (filled squares) and vertical (filled circles) beam radii at which the electric field is 1/e of the peak value as functions of distance from the guide end compared to the theoretical waists for the three gyrotrons. The measured beam radii agree quite well with the theoretical values, so well that it is difficult to distinguish the measured horizontal and vertical radii, which are nearly identical to each other, indicated on the plot.

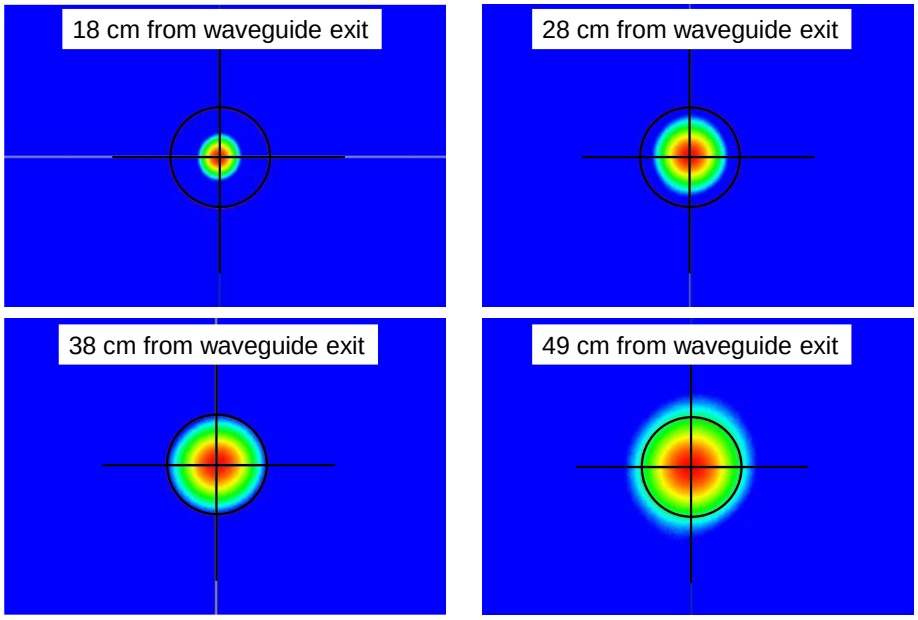

Fig. 8 Infrared images of the 527*GHz* gyrotron output beam. The crosshairs represent the position of the waveguide center and the circle is 5.08*cm* in diameter. The target distance from the corrugated waveguide exit is indicated on each image.

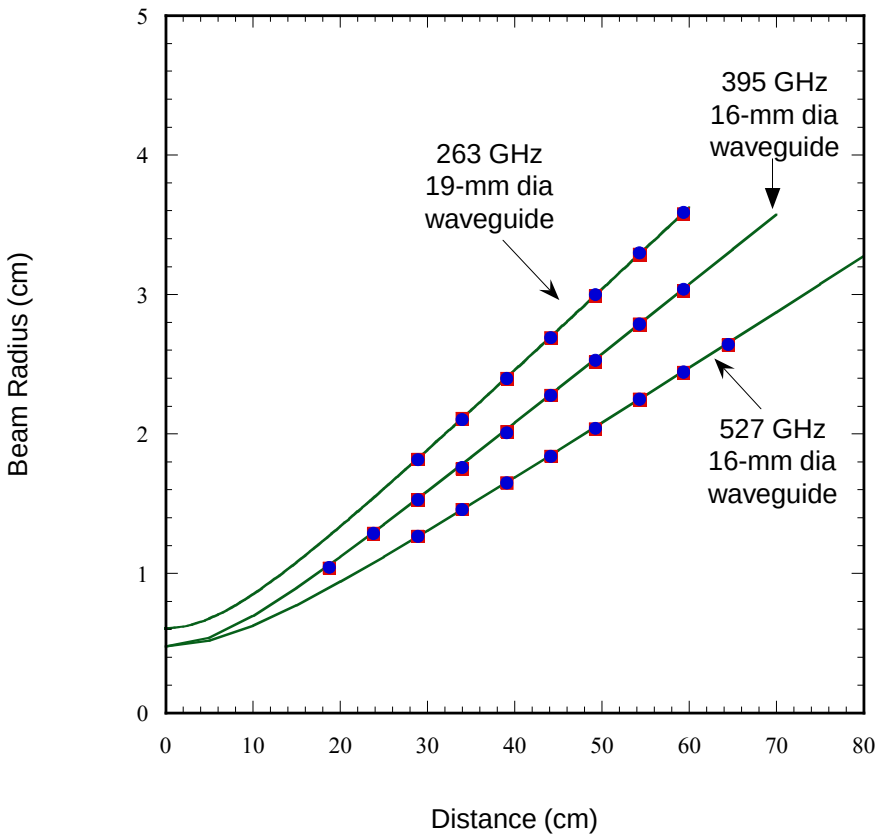

Fig. 9 Theoretical and measured beam radii as a function of distance for the output beams from the 263*GHz*, 395*GHz*, and 527*GHz* gyrotrons. For each of the three, the solid line shows the theoretical beam radii, the filled squares show the measured horizontal radii, and the filled circles show the measured vertical radii.

Mathematical modal decompositions of the measured beam profiles show, typically, greater than 95% overlap between the measured beams and an ideal Gaussian beam from a 19*mm* diameter (263*GHz*) or 16-*mm* diameter (395*GHz* and 527*GHz*) corrugated waveguide.

In addition to parameter variation curves and infrared images of the output beam, several other tests intended to demonstrate the gyrotron's stability and reliability are typically performed. The long-term stable operation of the gyrotron is demonstrated, wherein the gyrotron is operated without fault continuously for greater than 72 *hours* with less than 1*MHz* frequency variation and less than 0.3*W* power variation over the run period. Also, operation at the nominal output power with 100% reflection is demonstrated by putting a piece of copper at the end of the waveguide. The gyrotron is then operated at the nominal point with 100% reflection for at least one hour without fault or damage.

4. Summary

In cooperation with Bruker, CPI has designed, developed, and demonstrated cw gyrotrons capable of producing at least 50*W* output power at 263*GHz*, 395*GHz*, and 527*GHz*. All three gyrotrons operate at the second harmonic of the cyclotron frequency. Each gyrotron is tested to demonstrate the power variation capabilities with varying beam voltage, beam current, and other parameters. In addition, infrared images are used to quantify the characteristics of the output beam and determine the Gaussian content.

To date, 30 DNP/NMR systems with CPI gyrotrons are installed and operating at Bruker customer sites. Bruker has delivered thirteen 400*MHz* spectrometers using the 263*GHz* gyrotron, twelve 600*MHz* spectrometers with 395*GHz* gyrotrons, and five 800*MHz* gyrotrons with 527*GHz* gyrotrons.

DNP-enhanced NMR spectroscopy promises to be an important and growing application for high-frequency cw gyrotrons.

Fig. 10 Photograph of an installed 527*GHz*/800*MHz* DNP/NMR spectrometer installed at a Bruker customer site.

References

[1] L.R. Becerra, G.J. Gerfen, R.J. Temkin, et al. "Dynamic nuclear polarization with a cyclotron resonance maser at 5 T". *Phys. Rev. Lett.*, 71, 3561-3564 (1993).

[2] L.R. Becerra, G.J. Gerfen, B.F. Bellew, et al. "A spectrometer for dynamic nuclear polarization and electron paramagnetic resonance at high frequencies". *J. Magn. Reson.* A, 117, 28-40 (1995).

[3] M.K. Hornstein, V.S. Bajaj, R.G. Griffin, et al. "Continuous-wave operation of a 460 GHz second harmonic gyrotron oscillator". *IEEE Trans Plasma Sci*, 34, 524-533 (2006).

[4] Y. Matsuki, H. Takahashi, K. Ueda, et al. "Dynamic nuclear polarization experiments at 14.1T for solid-state NMR". *Phys. Chem. Chem. Phys.*, 12, 5799–5803 (2010).

[5] S. Alberti, J. Ph. Ansermet, F. Braunmuller, et al. "Experimental results on a modular gyrotron operating at 0.26 THz for 400 MHz DNP/NMR spectroscopy applications". 38th Int. Conf. on Infrared, Millimeter. and Terhertz Waves (IRMMW-THz 2012), Woolongong, Australia, Sept 23-28, Thu-A-2-3 (2012).

[6] S. Jawla, Q.Z Ni, A. Barnes, et al., "Continuously tunable 250 GHz gyrotron with a double disk window for DNP-NMR spectroscopy". J. Infrared Milli Terahz Waves, 34, 42-52 (2013)

[7] R. Ikeda, Y. Yamaguchi, Y. Tatematsu, et al. "Broadband continuously frequency tunable gyrotron for 600 MHz DNP-NMR spectroscopy". *Plasma Fusion Res.*, 9, 1206068 (2014)

[8] T. Idehara, Y. Tatematsu, Y. Yamaguchi, et al. "The development of 460 GHz gyrotrons for 700 MHz DNP NMR spectroscopy". *J. Infrared Milli Terahz Waves*, 36, 613-627 (2015).

[9] V. Denysenkov, M.J. Prandolini, M. Gafurov, et al. "Liquid-state DNP using a 260 GHz high power gyrotron". *Phys. Chem. Chem. Phys.* 12, 5786-5790 (2010).

[10] M.Yu. Glyavin, A.V. Chirkov, G.G. Denisov, et al. "Experimental test of a 263 GHz gyrotron for spectroscopic applications and diagnostics of various media". *Rev. Sci. Instrum.* 86, 054705 (2015).

[11] M. Rosay, L. Tometich, S. Pawsey, et al. "Solid-state dynamic nuclear polarization at 263 GHz: spectrometer design and experimental results". *Phys. Chem. Chem. Phys*. 12, 5850-5860 (2010).

[12] A. A. Bogdashov, A. V. Chirkov, G. G. Denisov, et al. "High-Efficient Mode Converter for ITER Gyrotron". *Int J Infrared Millimeter Waves*, 26, 771-785 (2005).